Influence of Task Constraints and Device Properties on Motor Patterns in a Realistic Control Situation

Hugo Loeches de La Fuente, Laure Fernandez, Jean-Christophe Sarrazin, Eric Berton, Guillaume Rao

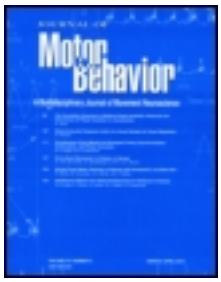

Journal of Motor Behavior
Publication details, including instructions for authors and subscription information:
http://www.tandfonline.com/loi/vjmb20

Influence of Task Constraints and Device Properties on Motor Patterns in a Realistic Control Situation

Hugo Loeches De La Fuente [a], Laure Fernandez [a], Jean-Christophe Sarrazin [b], Eric Berton [a] & Guillaume Rao [a]

[a] Aix-Marseille Université, CNRS, ISM UMR 7287, 13288, Marseille cedex 09, France

[b] Office National d'Etudes et de Recherches Aérospatiales, Département Commande des Systèmes et Dynamique du vol (DCSD), Salon de Provence, France

Published online: 28 Oct 2013.

To cite this article: Hugo Loeches De La Fuente, Laure Fernandez, Jean-Christophe Sarrazin, Eric Berton & Guillaume Rao, Journal of Motor Behavior (2013): Influence of Task Constraints and Device Properties on Motor Patterns in a Realistic Control Situation, Journal of Motor Behavior, DOI: 10.1080/00222895.2013.837424

To link to this article: http://dx.doi.org/10.1080/00222895.2013.837424

Journal of Motor Behavior, Vol. 46, No. 1, 2014

RESEARCH ARTICLE

Influence of Task Constraints and Device Properties on Motor Patterns in a Realistic Control Situation

Hugo Loeches De La Fuente[1], Laure Fernandez[1], Jean-Christophe Sarrazin[2], Eric Berton[1], Guillaume Rao[1]
[1]Aix-Marseille Université, CNRS, ISM UMR 7287, 13288, Marseille cedex 09, France. [2]Office National d'Etudes et de Recherches Aérospatiales, Département Commande des Systèmes et Dynamique du vol (DCSD), Salon de Provence, France.

ABSTRACT. The influences of task difficulty (index difficulty: 2–4), input device of different length, range of motion and mode of resistance (joystick or rotorcraft stick), and directions of movement (leftward rightward) on motor patterns in a realistic control situation were examined with a multilevel analysis (joint kinematics and muscular variables, and global task performance). Eight subjects controlled the displacements of a virtual object during a slalom task characterized by a realistic inertial model. Pilots adapted the endpoint kinematic organization to increasing accuracy constraints to preserve task success whatever the device and the direction. However, the rotorcraft stick manipulation remains highly complex in comparison to the joystick due to poorer proprioceptive information, higher inertial constraints, and an asymmetrical muscle control.

Keywords: biomechanics, human-computer interaction, motor control, multilevel analysis, speed-accuracy trade-off

Most tasks in human-computer interactions, from pointing an item with a joystick to piloting with a rotorcraft stick, involve speed and accurate movements in order to interact with the environment. To achieve these goals in various contexts of interaction, the CNS has to face constraints both in effector space (space where the device of interaction with the environment, such as a joystick, is manipulated) and in task space (space where the task is defined such as the screen of a computer in a video game or the visual environment in a rotorcraft cockpit).

Constraints in task space require adapting movement duration with movement accuracy requirements (Fitts, 1954). Thus, while pointing as fast as possible, the speed of execution will be kept to the detriment of the final precision. Conversely, the more precision required, the more the speed of execution will be compromised. This phenomenon is called the speed-accuracy trade-off and Fitts formalized this relationship by the law $MT = a + b \times Log_2(2D/W)$, where MT is the movement time, and D and W are the distance between targets and target width, respectively. $Log_2(2D/W)$ is the index of difficulty (ID), which quantifies the level of difficulty of the pointing task (Fitts, 1954; Fitts & Peterson, 1964) that characterizes the adapted movement in task space and a and b are empirical constraints.

MT depends on the kinematic organization of the endpoint effector movement required to face to difficulty level while pointing as fast as possible. Some authors highlighted the effect of ID on the organization of movement in reciprocal Fitts' tasks[1] (Fernandez & Bootsma, 2004, 2008; Mottet & Bootsma, 1999). Easy reciprocal aiming (low IDs) presents a harmonic or sinusoidal feature (smooth trajectory), with a bell-shaped velocity profile. However, as the difficulty of the task increases, the kinematic pattern looses its sinusoidal characteristics, with the peak of velocity occurring earlier, resulting in a longer deceleration phase. Thus, when ID increases, the subjects spent more time adjusting their movement based on sensory feedback while approaching the targets.

In the effector space, humans must select their movements appropriately not only to face to the spatial accuracy requirements in the task space but also in accordance with the constraints inherent to the manipulation of a specific device. Baird, Hoffmann, and Drury (2002) investigated the effects of probe length on MT in a discrete Fitts' task and reported that an increased probe length had a deleterious effect on MT. These authors also revealed a significant interaction between probe length and ID with a greater influence of probe length on MT for higher IDs. Consequently, the influence of devices properties would have a more severe influence when facing high accuracy requirements. Bongers, Smitsman, and Michaels (2003) investigated how device properties affect multijoint reaching actions and demonstrated that varying both length and mass properties of a pointing rod may create new postural constraints. That is, the participants selected a reaching distance that both accommodates the length of the rod and allows for a posture with which the rod can be controlled. These authors suggested that their findings can be generalizable to manual pointing and reaching movements as well as to movements involving many tools of daily usage (e.g., pens, needles, screwdrivers, oil dipsticks).

The resistance mode of the device could also influence the organization of movement when controlling the end effector. Zhai (1995) sorted devices as elastic or isotonic based on the different resistance modes. Elastic devices can be moved in a determined direction, with a spring applying a force opposite to the handle displacement. One example of elastic device is the two degrees of freedom (DoF) joystick that is widely used for video games. Contrary to elastic devices, isotonic devices are free moving (e.g., rotorcraft sticks where the resistance is independent of the displacement).

The particularity of joysticks as well as rotorcraft sticks is that the user controls the angular displacements (end-effector

Correspondence address: Hugo Loeches De La Fuente, Institut des Sciences du Mouvement, Faculté des sciences du sport, Aix-Marseille Université, 163 Avenue de Luminy 13009 Marseille, France. e-mail: hugo.loeches-de-la-fuente@univ-amu.fr

displacements) from one position to another by organizing movement within a closed kinematic chain. The mechanical linkage of the upper limb and the device forms this closed kinematic chain. In this particular case corresponding to several working situations such as industrial control, aviation, or surgical robotics, the movement is produced within the space of its possible solutions regarding the shaft length and the physical range of motion. To our knowledge, while elastic and isotonic devices are suggested to provide different kinesthetic information (Zhai, 1995), little is known about the effect of resistance mode combined with the device physical properties (i.e., shaft length and angular range of motion) on the organization of accurate movement when controlling end-effector displacements.

The speed-accuracy trade-off is generally presented as the consequence of an optimal behavior in effector space to guarantee the success in task space. Pointing as fast and as accurately as possible corresponds to MT and movement end-effector variance minimization (Guigon, Baraduc, & Desmurget, 2008; Harris & Wolpert, 1998; Meyer, Abrams, Kornblum, Wright, & Keith Smith, 1988; Tanaka, Krakauer, & Qian, 2006). Rancourt and Hogan (2001) postulated that the stiffness of the upper limb could play an important role in stabilizing the end-effector displacements. Several studies demonstrated that muscle coactivation (simultaneous activation of agonist and antagonist muscles around a joint) is needed to change the upper limb stiffness (Hogan, 1984; Milner, 2002; Milner & Cloutier, 1993). Indeed, coactivation provides the nervous system a way to adapt the mechanical properties of the limb to the task constraints during movement (Gribble, Mullin, Cothros, & Mattar, 2003; Osu et al., 2004; Selen, Beek, & van Dieën, 2006). Gribble et al. brought evidences of a relationship between coactivation and movement accuracy in multijoint limb movements. They observed an inverse relationship between target size and coactivation: when movement time was prescribed, coactivation increased as target size was reduced. In addition, end-effector accuracy improved. This suggests that, although energetically expensive, coactivation may be a strategy used by the motor system to improve limb stability and facilitate multijoint arm movement accuracy (Gribble et al., 2003; Laursen, Jensen, & Sjogaard, 1998; Osu et al., 2004; Selen et al., 2006; Visser, De Looze, De Graaff, & Van Dieën, 2004; Wong, Wilson, Malfait, & Gribble, 2009). To our knowledge, the modulation of muscle coactivation has been widely investigated in discrete pointing task but is still unknown for successive fast and accurate movements involved in human-computer interaction tasks such as piloting with an input device.

Most of the last situations cited previously require controlling arm movement in different directions when manipulating an input device while taking into account constraints in the task space (e.g., target position, obstacle). Furthermore, for each direction, movement is also submitted to constraints in effector space due to specific anatomical characteristics. However, Oel, Schmidt, and Schmitt (2001) reported no differences between left-to-right and right-to-left movements on MT when performing a mouse-based pointing task. However, the investigation of the global influence of the direction of movement on both the motor behavior (i.e., muscle control and joint kinematics) and on the kinematic organization of movement is needed and would provide a better understanding of the resulting behavior.

In the present study, we investigated the motor patterns in a realistic control situation that requires facing constraints encountered in most human computer interactions tasks. The participants had to control fast and accurate displacements of a virtual object (i.e., rotorcraft or vehicle) whose physical behavior was simulated by a dynamical model. We examined the effects of the ID, the input device manipulated (device), and the direction of movement on end-effector kinematic pattern, kinematic pattern of the virtual object controlled on the screen, joint kinematics, and muscle activity. We hypothesized that increasing accuracy constraints (i.e., ID) would induce a loss of the sinusoidal characteristics of the kinematic patterns in effector and task spaces resulting in an increase of MT. Whatever the device controlled, we also expected an effect of an increasing ID on muscle control with an increase of muscle coactivation. Besides, we hypothesized that the participants would adapt joint kinematics and MT to each device in order to preserve task success. Then, we hypothesized that there will be no effect of the direction of movement (right or left) on MT.

Method

An aiming task carried out in an egocentric frame of reference was proposed to the participants. Participants had to control a virtual object with an input device in a virtual environment in order to pass through successive doors as quickly as possible. Two different input devices were tested: a joystick and a rotorcraft stick. We considered both the displacements of the object and the participant's motor behavior. The displacements of the object and the participant's motor behavior (displacements of the input device, electrical activity of the muscles, and joint kinematics) were recorded during the task for four different IDs. The virtual environment where the task was defined and in which the object moved is referred to as the task space while the space in which the participant's upper limb moved is the effector space. Task space and effector space constituted two separate and complementary levels of analysis providing a global survey of the influence of devices properties, task difficulties, and movement directions on the motor patterns.

Participants

Participants were eight right-handed helicopter pilots (eight men; M age $= 22$ years, $SD = 1.18$ years). All participants had no previous history of upper extremity musculoskeletal disorders and all reported normal or corrected to normal vision. All participants were experienced computer users and had experience with flight simulators.

Tasks

The participants performed the task by using an input device to control the displacements of the object in the virtual environment. The virtual object displacements were controlled along two orthogonal axes (medialateral and longitudinal axes) in the horizontal plane while the vertical movement was not controlled. We introduced dynamical relationships between the displacement of the input device in the effector space and the displacements of the object in the task space. This dynamical model is mimicking the physical behavior of a moving object. The dynamical model will be further detailed in the experimental setup section.

The participants were asked to cross successively and as quickly as possible 22 doors presented in the virtual scene. The trial was rerun if participants did not succeed in performing the slalom task with less than 25% of missed doors until the criterion was met. The effective mean rate of missed doors during the experimentation was 14.93%. A 1-min rest between each trial (successful or not) was respected.

The experimentation contained two successive phases: a familiarization phase and an experimental phase. During the familiarization phase the participants became familiar with the virtual environment and the use of the input device to control the object in the presence of the dynamical model. The participants were considered as familiarized when they were able to succeed at least one trial for each ID condition and for each input device. When the participants were familiarized with the apparatus and the virtual environment, the experimental phase started.

Experimental Design

The experimentation contained two sessions. Each session was characterized by the use of one of the two different input devices. The first input device was a two DoF joystick (Extreme 3D Pro, Logitech, Fremont, CA) and the second input device was a two DoF helicopter rotorcraft stick (G-Stick III Plus, FlightLink, Chico, CA). The joystick was an elastic pointing device, where resistance increased with displacement while the rotorcraft stick was an isotonic input device with free-moving displacements. Besides, the shaft length of the rotorcraft stick (57 cm) was longer than the shaft length of the joystick (15 cm). The sticks rotated about two orthogonal axes defined in the horizontal plane (i.e., the medialateral axis and longitudinal axis). These two axes of rotation of the sticks corresponded to the two orthogonal axes of displacement of the virtual object defined in the horizontal plane in task space. Besides, the angular range of motion of the joystick and the rotorcraft stick were respectively equal to 40° and 20° about each axis. Taken together, these physical characteristics leaded to ranges of tip motion in the horizontal plane along both the longitudinal and the medialateral axes of 10 cm and 20 cm respectively for the joystick and the rotorcraft stick.

In order for the two devices to provide comparable outputs, the output value of the angular position was normalized to be included within the interval [–1, +1] for each axis of displacement while a zero was set when the device returns to its upright position.

Within each session, each condition was characterized by a quantified ID. ID = $\log_2$(2D/W), where D is the distance between the center of two successive doors (Figure 1) along the medialateral axis and W is the interdoors distance (i.e., the tolerance of the spatial precision). Four widths (3.20, 2.22, 1.63, and 1.25 m) and one distance D (10.00 m) were prescribed. Combinations of W and D gave rise to a total of four conditions with ID ranging from 2.5 to 4 bits (with a 0.5 bit increment).

The experimental phase was constituted by six trials for each of the different ID conditions. The order of the devices employed and the order of the conditions for each device were randomized to avoid any learning effect.

Experimental Setup

The experimental setup was used to record the virtual object position in the task space and the participant's motor behavior including the position of the input device, the joint kinematics of the upper limb segments, and the muscle electromyographic activity (EMG).

Task Space

We simulated in real time a three-dimensional environment in which a virtual object was driven with a realistic physical behavior taking into account the object mass and air resistance. This environment was simulated with a software program (COLOSSE) developed in the ONERA DCSD laboratory and running on a computer. The virtual environment (task space) presented the successive doors (Figure 1). The ground texture had the appearance of sand and mountains were presented in the scene background.

The proposed dynamical model was used to simulate the physical behavior of an object in real situation, such as, for example, a low altitude flight operation in helicopter or video gaming. Hence, in the task space, the object that was characterized by a mass could move in the presence of external forces. External forces were applied on the object when the participant displaced the input device in the effector space. The displacements of the object were thus characterized by a dynamical model simulating both inertia and air resistance (drag). This dynamical model is described by

$$\sum_i \vec{F} = m\vec{a} \quad (1)$$

Where $\vec{F}_i$ is the external force exerted on the object and m is the mass of the object ($m = 94$ kg). In this study the object of reference was an unmanned aerial vehicle (UAV), and $\vec{a}$ corresponds to the acceleration of the center of mass of the object.

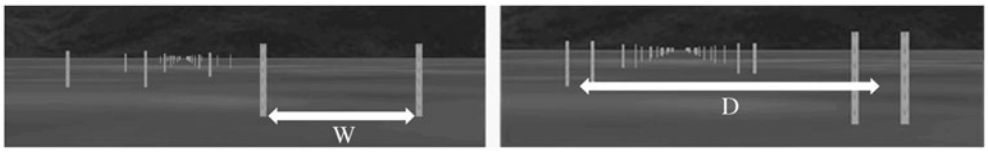

FIGURE 1. Task space visualization representing the successive doors in the virtual environment. D is the distance between the center of two successive doors and W is the interdoor distance. The parameter W was tuned to obtain different index of task difficulty. The left panel represents the lowest index of task difficulty (ID; 2.5 bits) and the right panel represents the highest ID (4 bits).

With

$$\sum_i \overrightarrow{F_i} = \overrightarrow{F_A} - \overrightarrow{F_D} \quad (2)$$

Where $\overrightarrow{F_A}$ is the force of advancement given to the object depending on the angular position (θ) of the input device along each axis (medialateral and longitudinal axes). The relationship between the angular position of the input device and $\overrightarrow{F_A}$ along each axis was linear with $\overrightarrow{F_A}$ being proportional to angular position in the effector space. This relationship was formalized by

$$\overrightarrow{F_A} = \begin{pmatrix} F_{ax} \\ F_{ay} \end{pmatrix} = k \begin{pmatrix} \theta_x \\ \theta_y \end{pmatrix} \quad (3)$$

where F_{ax} is the force of advancement on the longitudinal axis, F_{ay} is the force of advancement on the medialateral axis, θ_x is the angular position of the input device around the medialateral axis, θ_y is the angular position of the input device around the longitudinal axis, k represents the control display. In the present experiment, k was set to 1. Because θ_x and θ_y were both normalized and bounded within the interval [–1, +1] for the joystick and the rotorcraft stick, F_{ax} and F_{ay} were also included within the interval [–1, +1] whatever the input device employed. Consequently, the normalization of the output angular position of each device and the use of the same control display (k) allowed us to compare the joystick and the rotorcraft stick in similar realistic condition of control.

$\overrightarrow{F_D}$, is the drag force, the force component in the direction opposed to the object velocity along each axis of displacement. The drag force is formalized by

$$\overrightarrow{F_D} = \begin{pmatrix} F_{dx} \\ F_{dy} \end{pmatrix} = \frac{1}{2}\rho A C_D \begin{pmatrix} v_x^2 \\ v_y^2 \end{pmatrix} \quad (4)$$

Where F_{dx} is the drag force on the longitudinal axis and F_{dy} is the drag force on the medialateral axis, v_x is the object velocity on the longitudinal axis and v_y is the object velocity on the medialateral axis. The velocities on each axe were scalar quantities in meters per second, ρ is the air density in kilogram per cubic meter, A is the reference area in square meters (area of the orthogonal projection of the object on a plane perpendicular to the direction of motion), and C_D is the dimensionless drag coefficient of the moving object. In the present experiment the product AC_D was equal to 0.254 representing the air penetration coefficient of the object (UAV).

Along each axis of displacement in the task space and for each time step, a double time integration was applied to the object acceleration data to obtain object position (Equations 5 and 6).

$$x(t) = \iint a_x(t)dt^2 \quad (5)$$

$$y(t) = \iint a_y(t)dt^2 \quad (6)$$

Where $x(t)$ is the virtual object position on the longitudinal lateral axis at the time t and $y(t)$ is the object position on the medialateral axis at the time t, $a_x(t)$ is the virtual object acceleration on the longitudinal axis at the time t, and $a_y(t)$ is the object acceleration on the medialateral axis at the time t.

As a consequence, the position of the object obtained from this dynamical model was not linearly proportional to the input device outputs.

The angular position of the input device around the longitudinal axis and the resulting position of the object on the medialateral axis were recorded at 75 Hz. The angular position of the input device around the longitudinal axis was further considered as the position in effector space and the medialateral position of the object was further considered as the position in task space.

The simulated environment was displayed on three connected LCD monitors (59.77 cm × 33.62 cm, 1920 × 1080 pixels resolution) with a horizontal field of view of 60° and a vertical field of view of 13°. The three monitors were positioned on a table in front of the participants at 150 cm from their trunk.

Effector Space

The participants were seated with their knees at 90° flexion. The location of the input device according to

participant's trunk was adjustable to take into account the anthropometric characteristics of each participant. For each input device held in its central position, the initial posture is described subsequently.

The joystick base was located on a table, the participants held the joystick in its central position with the shoulder in neutral position, the elbow flexed at 90°, the forearm pronated at 90°, and the wrist in neutral position (see the left illustration in Figure 2).

The rotorcraft stick base was located below the participant's seat, the participants held the rotorcraft stick in its central position with the shoulder at 30° of flexion and abduction, the elbow was fixed at 30° of flexion (full extension being 0°), and the wrist was in neutral position and the forearm was pronated at 90° (see the right illustration in Figure 2). This posture corresponds to a typical piloting configuration.

The two initial postures were selected to be representative of the use of each device in real working situations. In order to provide a maximal standardization of each device manipulation, we minimized the potential effect of the different initial configurations of upper extremity on proprioceptive information (Flanagan & Lolley, 2001) by setting common initial wrist joint angles conditions when the subjects held the device in its central position (0,0). Thus, subject were asked to hold the device with 0° of wrist flexion-extension and abduction-adduction and the forearm pronated at 90° in both cases.

Joint kinematics of the upper limb segments (wrist, elbow and shoulder joint angles) were recorded using an inertial gyroscopic system (IGS-190, Animazoo, Brighton, UK) at a 60 Hz frequency. The participants wore an inertial motion capture suit with three 3-axis gyroscopes. The gyroscopes were attached to the hand, the forearm, and the arm. The data from those three sources were integrated and combined online and joint angular data were thus directly recorded from the sensors.

The surface electromyographic activity of 10 muscles was recorded synchronously at 2000 Hz using a BIOPAC system (MP150, Biopac Systems, Goleta, CA) with Ag/Ag-Cl bipolar surface electrodes (Skintact model FS 501, Innsbruck, Austria) in order to obtain the relationships between the upper limb joint kinematics and activities of related muscles. In the present study each muscle was associated with a specific basic upper limb joint movement.

For the shoulder joint movements, we recorded the activity of the deltoideus medius (DM; shoulder abduction), the deltoideus posterior (DP; shoulder extension), the pectoralis major (PM; shoulder flexion/adduction), and the teres major (TM; shoulder adduction). In addition, we obtained the activity of muscles associated with elbow joint movements recording the activity of the biceps brachii (BB; elbow flexion) and the triceps brachii (TB; elbow extension). At last, for the wrist and radioulnar joint movements, we recorded the activity of the pronator teres (PT; forearm pronation), the brachioradialis (BR; forearm supination), the extensor carpi ulnaris (ECU; wrist ulnar deviation), and the extensor carpi radialis (ECR; wrist radial deviation). Electrodes placement and locations were suggested by the SENIAM recommendations (Hermens, Freriks, Disselhorst-Klug, & Rau, 2000). The reference electrode was fixed on the skin overlying the lateral epicondyle. The locations of electrodes are shown in Figure 3.

Maximum voluntary contractions (MVC) of each muscle were recorded before the familiarization phase. The subjects performed three MVCs of each previously mentioned muscle by contracting the muscles as intensely as possible against an isometric resistance for 3 s. For the BR, PT, ECU, ECR, and TB muscles, the participants were seated and used a fixed handle located on a table. They held the handle with the shoulder in neutral position, the elbow flexed at 90°, the forearm parallel to the table plane and the wrist in neutral position. Participants were instructed to force as much as possible on the handle in the directions corresponding to the muscular actions of the muscles (respectively to the right, to the left, forward, backward, and downward against the table). For the BB, PM, DP, TM, and DM muscles, the participants were standing and isometric contractions were produced by pulling on a rope that acted as a fixed resistance located on the floor. For BB, participants grasped the rope with the elbow flexed at 90°. The shoulder and the wrist were in neutral position. They were instructed to raise their forearm by flexing the elbow. For the PM, DP, TM, and DM muscles, participants grasped the rope with the forearm pronated at 90° and the elbow maintained in full extension. The shoulder and the wrist were in neutral position. They were instructed to raise their arm respectively in front of them, posteriorly, to the right and to the left. Verbal encouragements were given to ensure maximum effort. A 1-min rest was given between recordings.

All data (position of the object, the angular position of the input device, joint kinematics of the upper limb, and the EMG activity) were recorded by synchronizing the COLOSSE software program, the ANIMAZOO IGS-190 system, and the BIOPAC MP150 system.

Data Processing

Each trial resulted in 10 cycles in the task space. A cycle corresponded to the data recorded between three successive doors resulting in 60 cycles per condition. For each direction of movement, all the recorded data were processed in order to obtain a representative half-cycle for each participant, each device employed, and each condition (ID).

Position data were low-pass filtered at 2 Hz in the task space and at 0.5 Hz in the effector space using a zero time-lag second-order Butterworth filter (Matlab, version 8.0.0.783, The MathWorks, Natick, MA). Acceleration data were computed by deriving twice position against time in both the task and the effector space. In the task space, the medialateral object position was derived against time twice and in the effector space, the angular position of the input device around the longitudinal axis was derived against time twice. Position and acceleration half-cycles were rescaled within the interval

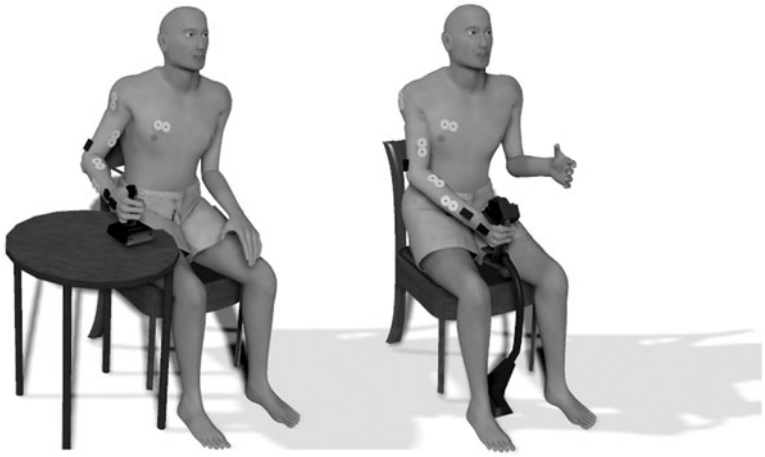

FIGURE 2. Effector space visualization for the manipulation of the joystick (left) and for the manipulation of the rotorcraft stick (right). Three gyroscopes and 11 surface electrodes (10 for each analyzed muscle and one for reference) were positioned on the right upper limb of the participant.

[–1, +1] and normalized in time (for details on method, see Mottet & Bootsma, 1999). From position signal in task and effector spaces, reversal points were then identified in order to distinguish right and left movement independently. Finally, the representative position and acceleration half-cycles were obtained in task and effector spaces by averaging the corresponding half-cycle profiles.

Joint kinematics signals were low-pass filtered (Butterworth second order, 3 Hz cutoff frequency). The reversal points of the position signal in effector space (i.e., angular position of the input device around the longitudinal axis) were used in order to distinguish right and left movement independently for each joint angle signal. Then the resulting half-cycle profiles were averaged to obtain a representative half-cycle.

Regarding the muscle activity data, for each data set (MVC and trials), EMG signals were band pass filtered from 20 to 400 Hz, full-wave rectified and low-pass filtered

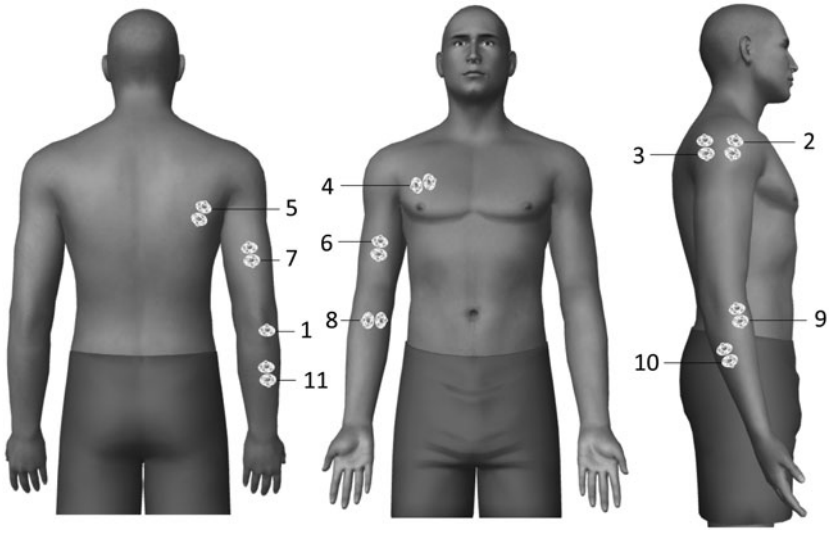

FIGURE 3. Locations of the EMG electrodes. 1 = reference electrode; 2 = deltoideus medius; 3 = deltoideus posterior; 4 = pectoralis major; 5 = teres major; 6 = biceps brachii; 7 = triceps brachii; 8 = pronator teres; 9 = brachioradialis; 10 = extensor carpi ulnaris; 11 = extensor carpi radialis.

(Butterworth second order, 6 Hz cutoff frequency). In order to allow comparison of the activity between specific muscles and the activity in specific muscles among different participants, the EMG signals were normalized (Kronberg, Németh, & Broström, 1990; Schüldt, Ekholm, Harms-Ringdahl, Arborelius, & Németh, 1987; Soderberg & Cook, 1983). For each participant and each muscle, EMG signals recorded during the experiment were divided by the maximum EMG value from the three processed MVCs. Thus, the EMG signal was expressed in percentage of the maximum EMG value. At last, for each normalized muscle activity, right and left movements were distinguished independently using the reversal points of the position signal detected in effector space. We obtained representative half-cycle of each muscle activity by averaging the resulting half-cycle profiles.

For each trial, a representative half-cycle was obtained for all the data. Thus we obtained a single representative half-cycle by averaging the six representative half-cycles. The dependent variables were computed from the average half-cycles for each device employed, each condition (ID), and each direction of movement whereas the relative Hilbert phase (see Dependent Variables section) was computed independently of direction of movement.

Dependent Variables

For the following dependent variables, the acronyms are respectively related to task or effector space through the last letter T or E.

In the task space, the different dependent variables were computed from the medialateral object position and acceleration. Movement time (MTT) was defined as the average half-cycle time of medialateral object position. Following segmentation of the movement based on movement reversals, MTT was calculated as the average time between two movement reversals.

The effective width of the target (W_e) was defined as 4.133σ where σ is the standard deviation of the actual endpoint distribution at movement reversal in task space. The index of performance (IP) was computed from MT and W_e using Equation 7 according the International Organization for Standardization standard recommendations (International Organization for Standardization, 2002). IP is recognized as a standard by academic and industry researchers for the evaluation of the performance when using a pointing device. IP was computed as:

$$IP = ID_e/MT \tag{7}$$

Where ID_e is the effective index of difficult adjusted by using effective width of the target is computed as

$$ID_e = \log_2\left(\frac{D}{W_e}+1\right) \tag{8}$$

Where D is the intertargets distance.

Harmonicity of movement (NPAT) was also measured in task space based on normalized peak acceleration values. The maximum normalized acceleration was computed for each half-cycle and was then averaged. NPAT yielded a sensitive measure indicating how close the pattern is to sinusoidal movement (Fernandez & Bootsma, 2004).

In the effector space, the different dependent variables were computed from the angular position and acceleration of the input device around the longitudinal axis, the joint kinematics and EMG data. Movement time (MTE) was computed from the input device angular position using the same method as in task space. The input device angular acceleration was used for the normalized peak of acceleration (NPAE) computation.

For the dependent variables related to muscle activity, the level of muscular coactivation was estimated using the wasted contraction (Gribble et al., 2003) measure. For each agonist-antagonist muscle pair (BR and PT, ECU and ECR, BB and TB, and PM-DM), we computed the wasted contraction at each sampling point and on the total duration of the half-cycle as

$$Wasted\ contraction(t) = \frac{Smaller\ trace(t)}{Maximum\ (Effective\ contraction)} \tag{9}$$

Where $Smaller\ trace(t)$ is the smaller normalized activity in each agonist-antagonist pair computed at the time t, $Effective\ contraction$ was computed as

$$Effective\ contraction(t) = Larger\ trace(t) - Smaller\ trace(t) \tag{10}$$

with $Larger\ trace(t)$ is the larger normalized activity in each agonist-antagonist pair computed at the time t.

$Maximum\ (Effective\ contraction)$ is the maximum value of effective contraction signal over the entire half-cycle.

Both maximal and minimal levels of this wasted contraction were estimated for each muscle pair. For the BR-PT, ECU-ECR, BB-TB, and PM-DM muscle pair, we respectively obtained BP_{min} and BP_{max}, EE_{min} and EE_{max}, BT_{min} and BT_{max}, and PD_{min} and PD_{max}.

Finally, for each DoF of each joint, the amplitudes of the joint kinematics were computed from the averaged half-cycle. The amplitude was computed as the difference between the maximal and the minimal value. We obtained SH_{aa}, SH_{fe}, and SH_{ie} for the abduction-adduction, flexion-extension, and internal rotation-external rotation of the shoulder, respectively. We obtained E_{fe} for the flexion extension of the elbow and F_{ps} for the pronation-supination of the forearm. We obtained W_{aa} and W_{fe} for the abduction-adduction and flexion-extension of the wrist, respectively.

At last, we investigated the phase coupling between movement in effector and task space. This phase coupling

informed us about the way the participants displaced the input device to control the virtual object displacements in the presence of the dynamical model. Thus we first computed the time-dependent relative Hilbert phase between movement in effector and task space (Huys, Daffertshofer, & Beek, 2004). The Hilbert phase is based on analytic signals (Gabor, 1946). In brief, the analytic signal $\zeta(t)$ is the complex extension of a time series, here denoted as $s(t)$, defined as $\zeta(t) = s(t) + is^*(t)$, where $s^*(t)$ is the time-series' Hilbert transform given by

$$s^*(t) = \frac{1}{\pi} PV \int_{-\infty}^{\infty} \frac{s(\tau)}{t-\tau} d\tau \qquad (11)$$

Where PV refers to Cauchy principal value. As for every complex-valued quantity, one can define amplitude and phase in terms of $\zeta(t) = A(t)\exp\{i\Theta_H)(t)\}$, so that $\Theta_H(t) = \arctan\{\Im[\zeta(t)]/\Re[\zeta(t)]\}$ represents the continuous Hilbert phase of the time-series $s(t)$. The relative Hilbert phase between two time-series $es(t)$ and $ts(t)$ is then defined as

$$\Delta\Theta_H(t) = \Theta_{H,es}(t) - \Theta_{H,ts}(t) \qquad (12)$$

Where es(t) and ts(t) are time-series of angular position of the input device around the longitudinal axis in effector space and medialateral object position in task space (e.g., see Pikovsky, Rosenblum, Osipov, & Kurths, 1997), respectively. Finally, we computed for each trial the mean value of the relative Hilbert phase (RHP) in order to quantify the effector space-task space phase coupling in degrees. We obtained RHP for each participant, each device employed, and each ID condition.

Statistical Analysis

Repeated measures analyses of variance (ANOVAs) were used to test the effects of device (i.e., joystick and rotorcraft stick), ID (i.e., 2.5, 3, 3.5, and 4) and direction of movement (i.e., right directed and left directed movements) on each dependent variable. In addition, we performed regression analyses on MTT and MTE to determine the degree of linearity as a function of ID. In order to verify that Fitts' law is retrieved in both effector and task space, we used pooled MTT and MTE across the two devices for such regression analyses. Significant effects were further characterized through a measure of effect intensity (EI) and Newman-Keuls post hoc tests were used when significance level ($p < .05$) was reached. Results with $.05 \leq p \leq .06$ were considered as tendencies to significance.

Results

Relative Hilbert Phase

The repeated measures ANOVA revealed significant main effects of ID, $F(3, 21) = 14.04$, $p < .05$, EI = 66.74%, on RHP (Figure 4) with higher RHP for IDs 3.5 ($174.28 \pm 0.24^\circ$) and 4 ($174.37 \pm 0.16^\circ$) than for IDs 2.5 ($174.10 \pm 0.28^\circ$) and 3 ($174.18 \pm 0.28^\circ$). No statistically significant effect of direction of movement or device on RHP was found.

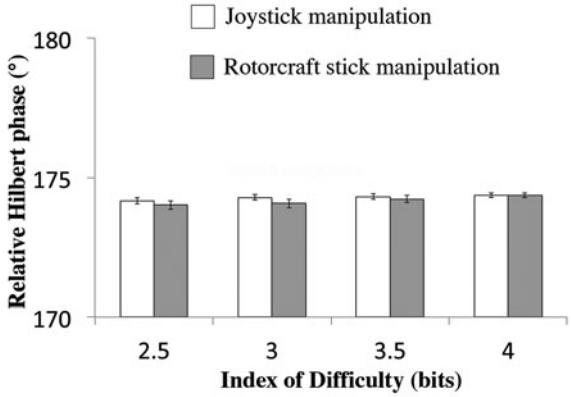

FIGURE 4. Mean relative Hilbert phase as a function of the index of difficulty for each session. The vertical bars indicate the standard deviation.

Movement Time

The regression analyses using MTT data indicated a linear relationship between MTT and ID ($R^2 = .99$). The regression analysis for effector space data also indicated a linear relationship between MTE and ID ($R^2 = .96$). MTT and MTE linearly increased with an increase of ID.

Effector Space

The analysis indicated a main effect of ID on the MTE, $F(3, 21) = 27.57$, $p < .05$, EI = 79.75%. Newman-Keuls test indicated higher MTE for IDs 3 (1.89 ± 0.15 s) and 3.5 (1.95 ± 0.19 s) than for ID = 2.5 while MTE was greater at ID = 4 (2.03 ± 0.19 s) than at other IDs (Figure 5). In addition, the main effect of device, $F(1, 7) = 50.60$, $p < .05$, EI = 87.85%, was significant with higher MTE obtained for the rotorcraft stick manipulation than for the joystick manipulation. No statistically significant effect of direction of movement on MTE was found.

Task Space

ANOVAs revealed significant main effects of ID, $F(3, 21) = 31.10$, $p < .05$, EI = 81.63%, on MTT. Newman-Keuls test on ID indicated that MTT for each ID was significantly different from all others (Figure 5). The main effect of device, $F(1, 7) = 114.84$, $p < .05$, EI = 94.25%, was also significant with higher MTT obtained for the rotorcraft stick manipulation than for the joystick manipulation. No

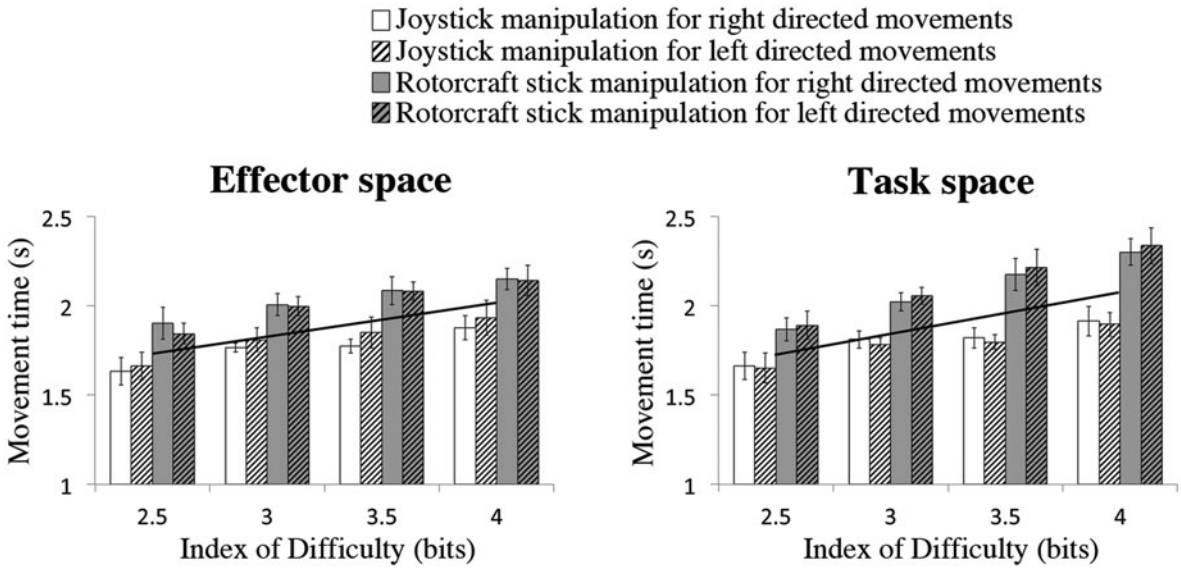

FIGURE 5. Movement time in effector space (left panel) and task space (right panel) as a function of the index of difficulty for each session and for the two directions of movement. The vertical bars indicate the standard deviation. The solid bold line represents the linear regression line.

statistically significant effect of direction of movement on MTT was found.

Normalized Peak of Acceleration

Effector Space

ANOVAs revealed significant device × direction of movement interaction for NPAE, $F(1, 7) = 14.73$, $p < .05$, EI = 67.78%. The decomposition of the interaction into simple effects first showed main effect of device on NPAE values with higher NPAE for the manipulation of the rotorcraft stick than for the manipulation of the joystick. The decomposition of the interaction also showed main effect of direction of movement on NPAE with higher NPAE for left-directed than for right-directed movements. The analyses of the interaction for NPAE demonstrated that the difference between right- and left-directed movements was higher for the manipulation of the rotorcraft stick than for the manipulation of the joystick. At last, the analysis detected a main effect of ID on NPAE, $F(3, 21) = 51.53$, $p < .05$, EI = 88.04%. Post hoc analyses revealed that NPAE for each ID was significantly different from all others (Figure 6). NPAE increased with task difficulty.

Task Space

The repeated measures ANOVA detected a significant device by direction of movement interaction for NPAT, $F(1, 7) = 10.32$, $p < .05$, EI = 59.59%. The decomposition of the interaction into simple effects first showed main effect of device on NPAT values with higher NPAT for the manipulation of the rotorcraft stick than for the manipulation of the joystick. The decomposition of the interaction also showed main effect of direction of movement on NPAT with higher NPAT for left-directed than for right-directed movements. The analyses of the interaction for NPAT revealed a greater difference between right- and left-directed movements for the manipulation of the rotorcraft stick than for the manipulation of the joystick. The analysis also detected a main effect of ID on NPAT, $F(3, 21) = 63.55$, $p < .05$, EI = 90.08%. Post hoc analyses revealed that NPAT for each ID was significantly different from all others (Figure 6). NPAT increased with task difficulty.

Effective Width of the Target

The analysis indicated a main effect of ID on W_e, $F(3, 21) = 27.55$, $p < .05$, EI = 79.74% (Figure 7). Post hoc analyses demonstrated that W_e was higher for ID 2.5 (0.44 ± 0.09 m) than for all other IDs. Furthermore W_e was higher for ID = 3 (0.40 ± 0.10 m) than for IDs 3.5 (0.34 ± 0.09 m) and 4 (0.33 ± 0.09 m). A significant effect of direction of movement on W_e, $F(1, 7) = 20.64$, $p < .05$, EI = 74.67% was also found with higher W_e for left-directed movements than for right-directed movements. At last, the analysis indicated a main effect of device on W_e, $F(1, 7) = 37.30$, $p < .05$, EI = 84.20%, with higher W_e for the rotorcraft stick manipulation than for the joystick manipulation.

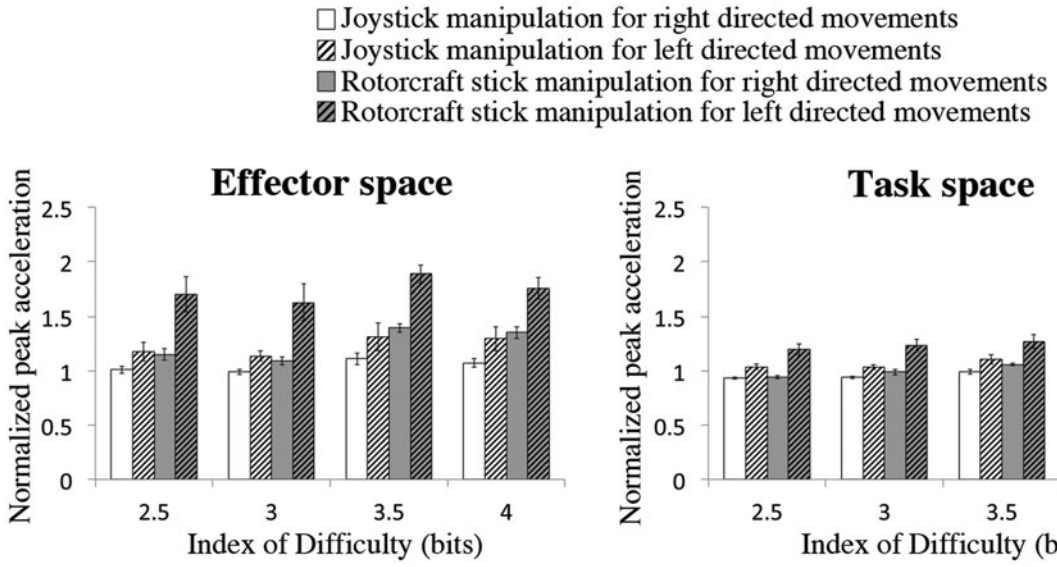

FIGURE 6. Normalized peak of acceleration in effector space (left panel) and task space (right panel) as a function of the index of difficulty for each session and for the two directions of movement. The vertical bars indicate the standard deviation.

Index of Performance

The repeated measures ANOVA revealed significant main effects of direction of movement on IP, $F(3, 21) = 19.63$, $p < .05$, EI = 73.72%. Newman-Keuls tests revealed higher IP for right-directed movements than for left-directed movements (Figure 8). In addition, the main effect of device on IP was significant, $F(3, 21) = 119.29$, $p < .05$, EI = 94.46%, with higher IP for the joystick manipulation than for the rotorcraft stick manipulation. No statistically significant effect of ID on IP was found.

Joint Angle Amplitude (Effector Space)

ANOVAs revealed a significant main effect of device on SH_{aa}, $F(1, 7) = 22.60$, $p < .05$, EI = 76.35%; SH_{fe}, $F(1, 7) = 7.97$, $p < .05$, EI = 53.25%; SH_{ie}, $F(1, 7) = 37.27$, $p < .05$, EI = 84.19%; and Fps, $F(1, 7) = 21.90$, $p < .05$, EI = 75.79%, where SH_{aa}, SH_{fe}, and S_{hie} were higher for the rotorcraft stick manipulation than for the joystick manipulation whereas F_{ps} was higher for the joystick manipulation than for the rotorcraft stick manipulation (Figure 9). In

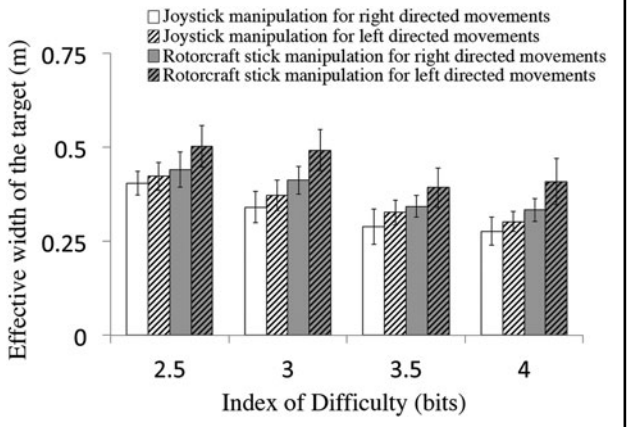

FIGURE 7. Effective width of the target in task space as a function of the index of difficulty for each session and for the two directions of movement. The vertical bars indicate the standard deviation.

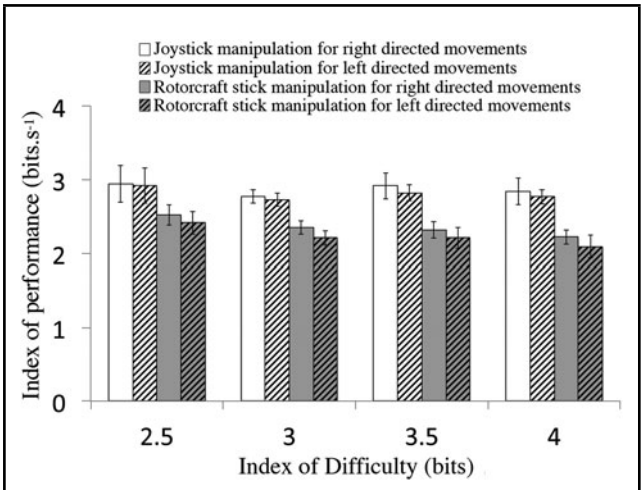

FIGURE 8. Index of performance in task space as a function of the index of difficulty for each session and for the two directions of movement. The vertical bars indicate the standard deviation.

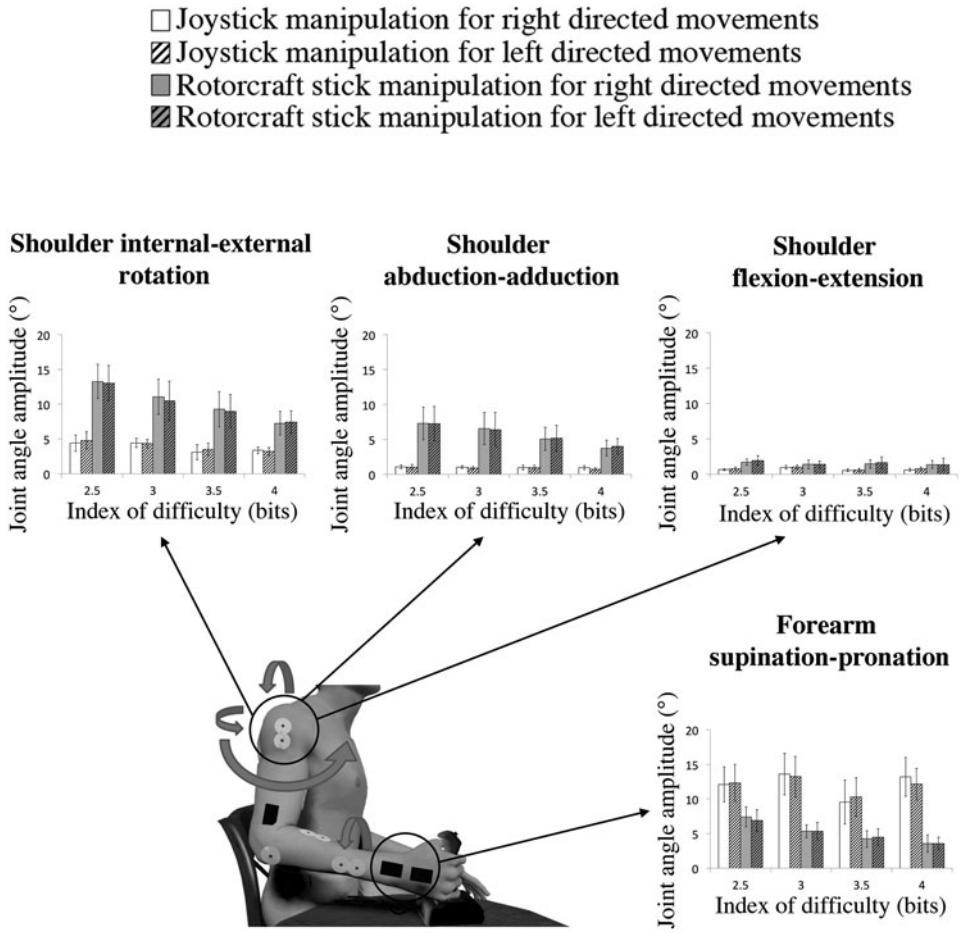

FIGURE 9. Joint angle amplitude in effector space as a function of the index of difficulty for each session and for the two directions of movement. The shoulder abduction-adduction, the shoulder flexion-extension, the shoulder internal rotation-external rotation, and the forearm pronation-supination are presented. The vertical bars indicate the standard deviation.

addition, the main effect of ID on SH_{ie} was significant, $F(3, 21) = 3.80$, $p < .05$, EI = 35.20%. Newman-Keuls test on ID factor indicated significant higher SH_{ie} for ID 2.5 ($8.57 \pm 5.61^{\circ}$) than for ID 4 ($5.46 \pm 3.10^{\circ}$). No statistically significant effect of direction of movement on joint angle amplitude was found.

Wasted Contraction

Minimal Level

The analysis detected a significant device by direction of movement interaction for PD_{min}, $F(1, 7) = 13.34$, $p < .05$, EI = 68.97%. The decomposition of the interaction into simple effects first showed main effect of device with higher PD_{min} values for the manipulation of the joystick than for the manipulation of the rotorcraft. The decomposition of the interaction also showed main effect of direction of movement with higher PD_{min} values for right-directed than for left-directed movements. The analyses of the interaction for PD_{min} revealed a greater difference between right- and left-directed movements for the manipulation of the rotorcraft stick than for the manipulation of the joystick (Figure 10). The analysis also detected a main effect of direction of movement on BT_{min}, $F(1, 7) = 9.14$, $p < .05$, EI = 56.63%, with BT_{min} values higher for right-directed than for left-directed movements. In addition, the main effect of device on EE_{min} was significant with higher EE_{min} for the joystick manipulation than for the rotorcraft stick manipulation. No statistically significant effect of ID on the minimal level of wasted contraction was found whatever the muscle pair considered but there was a tendency ($p = .06$) for PD_{min} to increase when ID increases.

Maximal Level

The analysis indicated a main effect of device on PD_{max}, $F(1, 7) = 6.45$, $p < .05$, EI = 51.80%, and on EE_{max}, $F(1, 7) = 7.13$, $p < .05$, EI = 50.47%, with both higher PD_{max} and

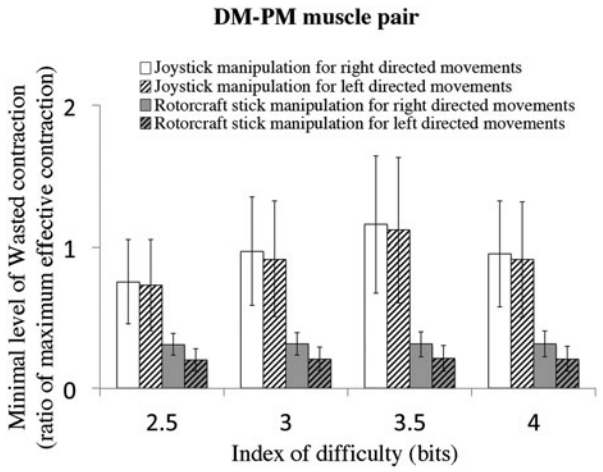

FIGURE 10. Minimal level of the wasted contraction of the agonist-antagonist muscle pair PM-DM in effector space as a function of the index of difficulty for each session and for the two directions of movement. The vertical bars indicate the standard deviation.

EE_{max} for the joystick manipulation than for the rotorcraft stick manipulation. ANOVAs also revealed main effect of direction of movement on BT_{max}, $F(1, 7) = 9.95$, $p < .05$, EI = 58.70%, with BT_{max} higher for right-directed than for left-directed movements. No statistically significant effect of ID on the maximal level of wasted contraction was found.

Discussion

The present study was aimed to investigate the motor patterns in a realistic control situation that requires facing constraints encountered in most tasks in human computer interactions. For this purpose, we examined the effects of the ID, the input device manipulated (device), and the direction of movement on end-effector kinematic pattern, kinematic pattern of the virtual object controlled on the screen, joint kinematics and muscle activity during a task mimicking a challenging piloting situation.

Our results demonstrate that Fitts' law can be retrieved in the task and effector spaces in presence of physical constraints (i.e., the dynamical model and the range of motion permitted by the device). As expected, an increase in ID, which was manipulated in the task space, induced a linear increase of movement time both in the effector and the task spaces ($R^2 = .96$ in effector space and $R^2 = .99$ in task space). Furthermore, larger values of NPAE and NPAT were reported when ID increased suggesting that ID also affected the kinematic patterns harmonicity. Thus, in line with earlier studies (Fernandez & Bootsma, 2004, 2008; Mottet & Bootsma, 1999), informational constraints in task space (i.e., ID) were found to have a strong effect on the kinematic organization of movement both in effector and task spaces: non-harmonic movements emerge for higher accuracy constraints (i.e., higher IDs), resulting in longer MTs. The particularity of the aiming task used in this study results from the use of realistic dynamical nonlinear relationships between the displacement of the device and the displacements of the virtual object (see Equations 1–6) that mimicked the physical behavior of the displaced virtual object (i.e., inertia or air resistance). Thus, while the mathematical relationship from the device medialateral position to the virtual object position is known (Equations 1–6), the resulting phase coupling between the effector and task spaces was investigated through the relative Hilbert phase. Our results demonstrated that positions through time in effector and task spaces were coupled in antiphase (RHP = 174.23 ± 0.23°) whatever the device manipulated and the direction of movement. Moreover, RHP was very slightly affected by ID (a difference of 0.27° between the mean values of RHP at ID 2.5 and 4). Participants thus controlled the object displacements in a direction in task space while producing a movement in the opposite direction in effector space preserving a constant optimal relationship between end-effector displacements and virtual object displacements. Interestingly, this antiphase control does not affect the linearity of the Fitts' law in both spaces, thus reinforcing its applicability in a wide range of situations.

Contrary to our expectations, movements that needed more accuracy at endpoint position (higher IDs) were not associated with higher levels of coactivation whatever the muscle pair considered. This last finding could be explained by the methodological differences between the present work and previous studies that investigated the level of coactivation for arm movements as a function of the accuracy constraints in a discrete aiming task (Gribble et al., 2003; Laursen et al., 1998; Osu et al., 2004; Visser et al., 2004). The task prescribed in previously cited studies consisted for the participants in pointing a target within a desired duration while the accuracy constraints (size of the target) were manipulated. In the present study, the participants were asked to cross as quickly and as accurately as possible the successive doors presented in the virtual scene while manipulating the accuracy constraints (interdoors distance). Consequently, the participants had to control both the speed and the accuracy of the displacements in the task space. Our results suggest that the participants selected their movements to minimize the negative consequences of biological noise. When interdoors distance was large, movement was produced with a high speed (low MTE) in effector space (i.e., with large motor commands), because the accuracy constraints of the task tolerated a large variability of the object reversal position in task space. When interdoors distance was small, movement speed had to be reduced in effector space (i.e., with smaller motor commands), so that variability of the virtual object position in task space remained within the door tolerance. In line with Missenard and Fernandez (2011), our results indicate that participants preferentially adapt movement speed to meet accuracy demands. The nervous system minimizes energy expenditure, thus emphasizing movement speed.

As expected, the device manipulated influenced movement time. Faster movements were reported in both task and effector spaces when the participants manipulated the joystick (1.79 ± 0.16 s in effector space and 1.79 ± 0.15 s in task space) than when they manipulated the rotorcraft stick (2.03 ± 0.17 s in effector space and 2.11 ± 0.22 s in task space). These results could arise from a combined effect of specific inertial constraints involving higher resistance to joint angular accelerations when manipulating the rotorcraft stick and a richer force and position feedback of the end-effector position when manipulating the joystick. Moreover, each device provides different kinesthetic information that could affect the control of the task by the subject. The joystick is a self-centering elastic device, where resistance increases with displacement and the rotorcraft stick is an isotonic device that is free moving. Zhai (1995) supposed that with an isotonic device, where movement is involved but not resistance, joint receptors, muscle spindles, and cutaneous receptors in the skin around the joints might contribute to proprioception in varying degrees. When using an elastic device as both movement and resistance are involved, the Golgi tendon organs may also contribute to the proprioception of hand action together with the former receptors. Specific initial configuration of the joint angles could also influence both muscles spindles and cutaneous afferents (Flanagan & Lolley, 2001). In the present work, setting common initial joint angles conditions when the subjects held the device in its central position minimized the respective influence of each device. The lower variability observed for the joystick manipulation could reveal that both proprioceptive and cutaneous inputs play an important role in the control of the endpoint position. Therefore, we suggest that the elastic joystick elicits response from more proprioceptors than the isotonic rotorcraft stick, because it allows movement while providing force feedback through the elastic elements. Our results are in line with those from Howland and Noble (1953) showing that subjects' performance was higher with the elastic device than with the isotonic device when studying time-on-target.

Beyond our expectations regarding the influence of device on the control of movement, the kinematic organization of motion was influenced by specific inertial constraints and proprioceptive feedback of end-effector position. Lower NPAE and NPAT where reported when manipulating the joystick than when manipulating the rotorcraft stick resulting in more harmonic kinematic patterns in both effector and task spaces for each level of task difficulty (Figure 6). The selected two devices are manipulated in real intensive working situations such as piloting operations. The joystick and the rotorcraft stick differed in their shaft length, angular range of displacement, and mode of resistance resulting in an influence of the device on the joint kinematics regardless the accuracy requirements. The participants manipulating the rotorcraft stick mainly mobilized the proximal joint (three DoF of the shoulder joint) to control the end effector whereas they mainly mobilized a distal two DoF system (wrist) and not the shoulder when manipulating the joystick. Higher shoulder joint amplitudes for two of the three DoF were observed in the manipulation of the rotorcraft stick (respective mean amplitude difference of 4.74° and 6.20° for the abduction-adduction and internal-external rotation of the shoulder between the two devices) while higher wrist joint amplitudes were reported in the manipulation of the joystick (mean amplitude difference of 6.71° for the forearm pronation–supination between the two sessions). The mobilization of the shoulder joint when manipulating the rotorcraft stick in the control of the end effector involves moving the whole upper limb whereas the mobilization of the wrist when manipulating the joystick involves rotating the forearm only. For each situation, the motion is submitted to specific inertial constraints due to mass distribution around the moving joints. These results clearly showed that the device properties influence the way the closed kinematic chain is organized and we suggest that the participants controlling the rotorcraft stick preserved task success by freezing the elbow joint. In line with the theory of Bernstein (1967) and more recent studies of human motor behavior (e.g., Newell, 1991; Vereijken, van Emmerik, Whiting, & Newell, 1992), this strategy would restrain the number of DoF mobilized entailing a radical simplification of the control of a complex multijoint closed

Fitts' (1954) performance model was chosen to examine the influence of input devices properties on the control of a virtual object. The resulting IP, a metric corresponding to an individual's capacity for executing a particular class of motor responses was computed from the effective interdoors distance (W_e) and MTT. As analysis revealed higher endpoint position variability under rotorcraft stick manipulation than for joystick manipulation as well as higher MTT in task space, we logically obtained much lower IP for the use of the rotorcraft stick. In the present study, because the total displacement of the tip of the stick along the medialateral axis is twice larger for the rotorcraft stick (20 cm) than for the joystick (10 cm), we could expect proportional differences in movement time in both effector and task space. It was however not the case (mean MT values across all IDs equal to 2.03 s in effector space and 2.11 s in task space for the rotorcraft stick and 1.79 s in effector space and 1.79 s in task space for the joystick) because of other factors influencing the participant's motor patterns. Thus, the combined influence of device physical properties and proprioceptive afferents provided by the device mode of resistance on the configuration of the closed kinematic chain results in specific inertial constraints due to mass distribution that contribute to influence movement time. This result summarizes the influence of the devices properties (physical characteristics and mode of resistance) on the control of movement in a realistic situation.

As expected the direction of movement (left–right movements along the lateral axis) did not influence MT whatever the levels of ID and the device manipulated. Henceforward, previous results on discrete task showing no difference with direction (Oel et al., 2001) can be extended to the reciprocal representation of Fitts paradigm under realistic conditions of control.

Direction of movement was however found to influence the activations of the muscles involved in the mobilization of the shoulder joint when controlling the rotorcraft stick (higher PD_{min} for right-directed than for left-directed movements). These results could be explained at a biomechanical level by the manipulation of the rotorcraft stick that requires performing shoulder abduction for right directed movement and a shoulder adduction for left directed movements. The shoulder abduction corresponds to an upward movement (with the medial deltoid acting concentrically against the gravity and the pectoralis major acting eccentrically) opposite to the shoulder adduction that corresponds to a downward movement facilitated by gravity (with the medial deltoid acting eccentrically). It was previously shown that the control of movements involving eccentric contraction requires a single muscle group and conversely that a concentric activation alone may not result in coordinated motions (Enoka, 1996). An asymmetrical control was reported with higher PD_{min} for right directed movements. This result could be attributed to the specific role of the agonist muscle group in the control of shoulder for opposite arm movement when controlling lateral end-effector displacements. In line with Enoka (1996), we found a higher minimal level of simultaneous activation of agonist and antagonist muscles when the shoulder is abducted in the manipulation of the rotorcraft stick than when the shoulder is adducted (only the eccentric muscle was solicited in this case). In opposition, the muscle activations for the joystick manipulation were symmetrical. In this case, the gravity acts symmetrically on the forearm and the direction of movement does not influence muscle control. Consequently, the muscle control of the rotorcraft stick, involving the control of a specific number of muscle groups regarding the direction of movement, seems more complex than the muscle control of the joystick. We suggest that this complexity contributed to increase the asymmetry of the kinematic organization of movement in both effector and task space. Interestingly, we also reported a device by direction of movement interaction showing that normalized peaks of acceleration (NPAE and NPAT) were more affected by the direction of movement when participants manipulated the rotorcraft stick than when they manipulated the joystick. This interaction could be explained by a higher minimal level of shoulder stability provided by the simultaneous activation of the PM-DM agonist-antagonist muscle pair for right directed movement ($PD_{min} = 0.31 \pm 0.16$ for right directed movement and $PD_{min} = 0.16 \pm 0.16$ for left directed movement) resulting in a higher degree of harmonicity of the kinematic pattern. This asymmetrical muscle control of the shoulder was also illustrated by the higher effective target width (W_e) for left directed movements than for right directed movements. Taken together, our results showed that global modifications of the kinematic organization of motion (W_e, NPAE, and NPAT) might be attributed to specific changes in the muscle activation patterns (changes in minimal levels of wasted contraction).

The main conclusion brought out by the present study is that the CNS specifically adapts the motor patterns to various constraints encountered in human computer interactions in order to preserve task success. Our results showed that the participants succeed the task in presence of nonlinear effector to task space relationships while adapting the endpoint kinematic organization for increasing accuracy constraints whatever the device manipulated and the direction of movement. We also evidenced a specific adaptation to the device manipulated with rotorcraft stick users facing physical properties constraint by mobilizing the shoulder and freezing the elbow and wrist joints. The consequence of this strategy is a simpler control of the closed kinematic chain by reducing the number of DoF mobilized. Moreover, it has been showed that the manipulation of the rotorcraft stick remains highly complex in comparison with the joystick. Indeed, the control of movement was subject to high inertial constraints due to mass distribution of the whole upper-limb around the shoulder joint. Then, the muscle control underlying the shoulder mobilization was complicated by an asymmetrical effect of gravity. The influence of both physical properties and resistance mode on the control of movement is summarized by a higher index of performance when manipulating a joystick than when manipulating a rotorcraft stick. A major contribution we have made in this study is to provide a global survey of the influence of the input device properties on the control of movement during realistic precision task (the object controlled was subjected to physical constraints of motion). Consequently, these results are not only theoretically interesting but also have practical significance when applied to the design of input devices that are used in working situation (e.g., gaming, robotic surgery, rotorcraft piloting).

NOTE

1. A reciprocal Fitts' task consists in pointing back and forth between two targets.

REFERENCES

Baird, K. M., Hoffmann, E. R., & Drury, C. G. (2002). The effects of probe length on Fitts' law. *Applied Ergonomics*, *33*, 9–14.

Bernstein, N. (1967). *The coordination and regulation of movements*. Oxford, England: Pergamon Press.

Bongers, R. M., Smitsman, A. W., & Michaels, C. F. (2003). Geometries and dynamics of a rod determine how it is used for reaching. *Journal of Motor Behavior*, *35*, 4–22.

Enoka, R. M. (1996). Eccentric contractions require unique activation strategies by the nervous system. *Journal of Applied Physiology*, *81*, 2339–2346.

Fernandez, L., & Bootsma, R. J. (2004). Effects of biomechanical and task constraints on the organization of movement in precision aiming. *Experimental Brain Research*, *159*, 458–466.

Fernandez, L., & Bootsma, R. J. (2008). Non-linear gaining in precision aiming: Making Fitts' task a bit easier. *Acta Psychologica*, *129*, 217–227.

Fitts, P. M. (1954). The information capacity of the human motor system in controlling the amplitude of movement. *Journal of Experimental Psychology*, *47*, 381.

Fitts, P. M., & Peterson, J. R. (1964). Information capacity of discrete motor responses. *Journal of Experimental Psychology*, *67*, 103.

Flanagan, J. R., & Lolley, S. (2001). The inertial anisotropy of the arm is accurately predicted during movement planning. *The Journal of Neuroscience*, *21*, 1361–1369.

Gabor, D. (1946). Theory of communication. *The Journal of the Institution of Electrical Engineers*, *93*, 429–457.

Gribble, P. L., Mullin, L. I., Cothros, N., & Mattar, A. (2003). Role of cocontraction in arm movement accuracy. *Journal of Neurophysiology*, *89*, 2396–2405.

Guigon, E., Baraduc, P., & Desmurget, M. (2008). Computational motor control: Feedback and accuracy. *European Journal of Neuroscience*, *27*, 1003–1016.

Harris, C. M., & Wolpert, D. M. (1998). Signal-dependent noise determines motor planning. *Nature*, *394*(6695), 780–784.

Hermens, H. J., Freriks, B., Disselhorst-Klug, C., & Rau, G. (2000). Development of recommendations for SEMG sensors and sensor placement procedures. *Journal of Electromyography and Kinesiology*, *10*, 361–374.

Hogan, N. (1984). Adaptive control of mechanical impedance by coactivation of antagonist muscles. *IEEE Transactions on Automatic Control*, *29*, 681–690.

Howland, D., & Noble, M. (1953). The effect of physical constraints on a control on tracking performance. *Journal of Experimental Psychology*, *46*, 353–360.

Huys, R., Daffertshofer, A., & Beek, P. J. (2004). Multiple time scales and multiform dynamics in learning to juggle. *Motor Control*, *7*, 188–212.

International Organization for Standardization. (2002). *Ergonomic requirements for office work with visual display terminals (VDTs)-Part 9: Requirements for non-keyboard input devices (ISO 9241–9). Reference Number: ISO 9241–9:2000(E)*. Geneva, Switzerland: Author.

Kronberg, M., Németh, G., & Broström, L. A. K. (1990). Muscle activity and coordination in the normal shoulder: An electromyographic study. *Clinical Orthopaedics and Related Research*, *257*, 76.

Laursen, B., Jensen, B., & Sjogaard, G. (1998). Effect of speed and precision demands on human shoulder muscle electromyography during a repetitive task. *European Journal of Applied Physiology and Occupational Physiology*, *78*, 544–548.

Meyer, D. E., Abrams, R. A., Kornblum, S., Wright, C. E., & Keith Smith, J. E. (1988). Optimality in human motor performance: Ideal control of rapid aimed movements. *Psychological Review*, *95*, 340.

Milner, T. E. (2002). Adaptation to destabilizing dynamics by means of muscle cocontraction. *Experimental Brain Research*, *143*, 406–416.

Milner, T. E., & Cloutier, C. (1993). Compensation for mechanically unstable loading in voluntary wrist movement. *Experimental Brain Research*, *94*, 522–532.

Missenard, O., & Fernandez, L. (2011). Moving faster while preserving accuracy. *Neuroscience*, *197*, 233–241.

Mottet, D., & Bootsma, R. J. (1999). The dynamics of goal-directed rhythmical aiming. *Biological Cybernetics*, *80*, 235–245.

Newell, K. M. (1991). Motor skill acquisition. *Annual Review of Psychology*, *42*, 213–237.

Oel, P., Schmidt, P., & Schmitt, A. (2001). Time prediction of mouse-based cursor movements. *Proceedings of Joint AFIHM-BCS Conference on Human-Computer Interaction IHM-HCI*, *2*, 37–40.

Osu, R., Kamimura, N., Iwasaki, H., Nakano, E., Harris, C. M., Wada, Y., & Kawato, M. (2004). Optimal impedance control for task achievement in the presence of signal-dependent noise. *Journal of Neurophysiology*, *92*, 1199–1215.

Pikovsky, A. S., Rosenblum, M. G., Osipov, G. V., & Kurths, J. (1997). Phase synchronization of chaotic oscillators by external driving. *Physica D: Nonlinear Phenomena*, *104*, 219–238.

Rancourt, D., & Hogan, N. (2001). Stability in force-production tasks. *Journal of Motor Behavior*, *33*, 193–204.

Schüldt, K., Ekholm, J., Harms-Ringdahl, K., Arborelius, U. P., & Németh, G. (1987). Influence of sitting postures on neck and shoulder emg during arm-hand work movements. *Clinical Biomechanics*, *2*, 126–139.

Selen, L. P. J., Beek, P. J., & van Dieën, J. H. (2006). Impedance is modulated to meet accuracy demands during goal-directed arm movements. *Experimental Brain Research*, *172*, 129–138.

Soderberg, G. L., & Cook, T. M. (1983). An electromyographic analysis of quadriceps femoris muscle setting and straight leg raising. *Physical Therapy*, *63*, 1434–1438.

Tanaka, H., Krakauer, J. W., & Qian, N. (2006). An optimization principle for determining movement duration. *Journal of Neurophysiology*, *95*, 3875–3886.

Vereijken, B., van Emmerik, R. E., Whiting, H. T. A., & Newell, K. M. (1992). Free (z) ing degrees of freedom in skill acquisition. *Journal of Motor Behavior*, *24*, 133–142.

Visser, B., De Looze, M. P., De Graaff, M. P., & Van Dieën, J. H. (2004). Effects of precision demands and mental pressure on muscle activation and hand forces in computer mouse tasks. *Ergonomics*, *47*, 202–217.

Wong, J., Wilson, E. T., Malfait, N., & Gribble, P. L. (2009). Limb stiffness is modulated with spatial accuracy requirements during movement in the absence of destabilizing forces. *Journal of Neurophysiology*, *101*, 1542–1549.

Zhai, S. (1995). *Human performance in six degree of freedom input control*. Doctoral dissertation, University of Toronto, Toronto, Canada.

Received April 23, 2013
Revised July 24, 2013
Accepted August 13, 2013